Available online at www.sciencedirect.com
ScienceDirect
Journal of Sound and Vibration 321 (2009) 8–25
JOURNAL OF SOUND AND VIBRATION
www.elsevier.com/locate/jsvi

Experimental validation of tonal noise control from subsonic axial fans using flow control obstructions

Anthony Gérard[a,*], Alain Berry[a], Patrice Masson[a], Yves Gervais[b]

[a]G.A.U.S., Mechanical Engineering Department, Université de Sherbrooke, Sherbrooke, QC, Canada JIK 2R1
[b]Laboratoire d'Études Aérodynamiques, Université de Poitiers, 86022 Poitiers Cedex, France

Accepted 11 September 2008
The peer review of this article was organised by the Guest Editor
Available online 31 October 2008

Abstract

This paper presents the acoustic performance of a novel approach for the passive adaptive control of tonal noise radiated from subsonic fans. Tonal noise originates from non-uniform flow that causes circumferentially varying blade forces and gives rise to a considerably larger radiated dipolar sound at the blade passage frequency (BPF) and its harmonics compared to the tonal noise generated by a uniform flow. The approach presented in this paper uses obstructions in the flow to destructively interfere with the primary tonal noise arising from various flow conditions. The acoustic radiation of the obstructions is first demonstrated experimentally. Indirect on-axis acoustic measurements are used to validate the analytical prediction of the circumferential spectrum of the blade unsteady lift and related indicators generated by the trapezoidal and sinusoidal obstructions presented in Ref. [A. Gérard, A. Berry, P. Masson, Y. Gervais, Modelling of tonal noise control from subsonic axial fans using flow control obstructions, *Journal of Sound and Vibration* (2008), this issue, doi:10.1016/j.jsv.2008.09.027.] and also by cylindrical obstructions used in the literature. The directivity and sound power attenuation are then given in free field for the control of the BPF tone generated by rotor/outlet guide vane (OGV) interaction and the control of an amplified BPF tone generated by the rotor/OGV interaction with an added triangular obstruction between two outlet guide vanes to enhance the primary non-uniform flow. Global control was demonstrated in free field, attenuation up to 8.4 dB of the acoustic power at BPF has been measured. Finally, the aerodynamic performances of the automotive fan used in this study are almost not affected by the presence of the control obstruction.

1. Introduction

Tonal noise from subsonic fans mainly originates from flow irregularity (non-uniform flow) that causes circumferentially varying blade forces and gives rise to a considerably larger radiated dipolar sound at the blade passage frequency (BPF) and its harmonics than a fan operating in a uniform flow. In many instances, axial fans operate in a non-uniform flow: this is the case of engine cooling fans that operate behind a radiator/condenser system or in the wake of inlet guide vanes [1].

*Corresponding author. Tel.: +1 819 821 8000x63161; fax: +1 819 821 7163.
E-mail address: Anthony.Gerard@USherbrooke.ca (A. Gérard).

0022-460X/$ - see front matter © 2008 Elsevier Ltd. All rights reserved.
doi:10.1016/j.jsv.2008.09.019

Nomenclature

a	circumferential Gaussian width parameter
a_R	radial Gaussian width parameter
B	number of blades
c_0	speed of sound ($m\,s^{-1}$)
C	chord of the blade (m)
D	harmonic content rate (%)
$\mathbf{H}$	aeroacoustic transfer matrix (m^{-2})
i	imaginary number $\sqrt{-1}$
J_n	ordinary Bessel functions, nth order
k_0	acoustic wavenumber, $k_0=\omega/c_0$ ($rad\,m^{-1}$)
$\tilde{L}$	unsteady lift (N)
L	amplitude of the unsteady lift (N)
N	number of discretized axial distance between the rotor and the obstruction
p	acoustic pressure (Pa)
R	radius (m)
R_H, R_T	fan hub and tip radii (m)
t	time (s)
w	circumferential order
W	sound power (W)
$\mathbf{x}; r, \varphi, \alpha$	acoustic field point coordinate; spherical coordinates
$\mathbf{y}; R, \theta, y_3$	acoustic source point coordinate; cylindrical coordinates
z_s	axial distance between the rotor and the obstruction
θ	circumferential angle (rad)
θ_s	angular position of the control obstruction (rad)
Θ	angle of the trapezoidal obstructions (deg)
ρ_0	density of air ($kg\,m^{-3}$)
σ	standard deviation
ω	angular frequency ($rad\,s^{-1}$)
Ω	angular velocity of the rotor ($rad\,s^{-1}$)

Subscripts and indices

m	acoustic frequency index
n	axial distance index
p	primary
s	secondary
t	total
T	tip

Superscripts

L	lift
opt	optimal

Techniques to control fan noise can be classified into two main families: active control or passive control. The latter has been extensively studied and has allowed tonal noise to be considerably reduced (see Ref. [2] for a synthetic state of the art). These methods are principally based on the geometrical characteristics of the propeller and its environment to reduce the generation mechanisms (reduce fluctuating forces or minimize their acoustic effects). Passive techniques can be classified as *preventive techniques*. However, when passive techniques have failed, active techniques have been proposed: Ref. [3] for automotive fans, Ref. [4] for PC cooling fans or Ref. [5] for ducted fans. The active techniques are also interesting since they are effective at low frequency, where passive techniques are inefficient (such as absorbing materials). They use the destructive interference between two waves: a secondary noise generated by a secondary source (loudspeaker for example) that interferes with the fan primary noise. These techniques can be classified as *corrective techniques*.

Another approach can however be pointed out: the cancellation of the acoustic source intensity due to non-homogeneous flow entering the fan, using a particular circumferential obstruction pattern. Theoretically, the circumferential pattern having the same number of lobes as the number of rotor blades (B) will emit intensive sound at the BPF (a mB lobed patter for the harmonic order m of the BPF). The concept is therefore to produce destructive interference between the primary source and an mB lobed obstruction (to control the harmonic m of the BPF). The control obstruction, must be located so that the secondary radiated sound is of equal magnitude but opposite in phase compared to the primary noise. If the primary non-uniform flow is stationary, the control obstructions location must be adapted only once. However, the control obstruction locations must be adaptive to control non-stationarity non-uniform flow. This research focuss on the control of the stationary part of the non-uniform flow.

Based on the technique suggested by Nelson [6], Kota and Wright [7] have proposed to radially insert independent upstream rods to experimentally introduce secondary non-uniformities into the flow. The steepest-descent algorithm has been implemented to automatically adjust the protrusion of one or more cylinders into the flow in order to minimize in-duct sound power. Experimental results show that, at low fan speed (only one duct mode was present), a 6 dB reduction is obtained at the BPF in far field, whereas a reduction of 8 dB and an increase of 5 dB are to be noted at $2 \times$ BPF and $3 \times$ BPF. At higher fan speed (three duct modes were present), a negligible reduction of 2 dB is obtained at the BPF.

Some other recent works have been conducted on this subject and reported in the literature. Recently, a control grid (wake generator) aimed at reducing rotor/stator interaction modes in fan engines when mounted upstream of the rotor has been studied [8]. Cylindrical rods were able to generate a spinning mode of the same order and similar level as the primary interaction mode. Mounting the rods on a rotating ring allowed for adjusting the phase of the control mode so that a 8 dB sound pressure level (SPL) reduction at the BPF was achieved when the two modes were out of phase. Since the wakes generated by the rods in Ref. [8] are salient, thus have a broad spectral content, the control of a tone affect the other tones. As an illustration, the results presented in the cited paper showed amplification of 6 and 15 dB for the first and second harmonics of the BPF respectively. Neuhaus et al. have also used cylindrical rods to control the BPF [9].

A patent [10] was filed recently which presents a technique and an apparatus based on sinusoidal circumferential variation of the tip clearance to create a unsteady pressure field opposite in phase with respect to the primary unsteady pressure field, thus reducing tonal noise. The proposed technique is based on sinusoidal variations of the inner surface of the shroud. Other patents related to the present work can be found in the literature, such as [11], which describe a method as well as a system to control tonal noise generated by a ducted-rotor. The method rely on the introduction of upstream or downstream flow distorsions to create an anti-sound opposite in phase with respect to the primary tonal noise. An acoustic signal from one or more microphone arrays provide information to adjust each circumferential modal component of the flow. Two methods for producing the distorsions are proposed. The devices are mounted in a circumferential array on the duct wall and consist of either (1) nozzles actively exhausting or ingesting controlled amount of air or (2) rods with actively controlled protrusion into the flow. Refs.[9,12] also propose steady air jets to reduce tonal noise in turbomachinery.

As opposed to what is reported in previous literature, the current work uses much more harmonically pure obstructions, which allows the control of a tone without affecting to the other tones. The goal of this paper is to characterize the acoustic performance of the flow control obstructions presented in Ref. [1] and to show that the obstruction designed to generate a low harmonic content rate is possible. An experimental assessment of the rotor/obstruction interaction and an indirect estimation of the harmonic content indicators proposed in Ref. [1], are first given in Section 2. Experimental acoustic directivity and sound power attenuation are then presented in free field in Section 3, using a sinusoidal obstruction geometry to control the primary noise arising from two flow conditions. Finally, the aerodynamic performance of the fan is experimentally evaluated with the flow control obstruction in Section 4.

2. Harmonic selectivity of the rotor/obstruction interaction

The harmonic selectivity performance of the obstructions is investigated in this section. The two harmonic content indicators proposed in Ref. [1] are indirectly estimated from acoustic pressure measurements in the axial direction of the fan thanks to the theoretical model presented [1].

2.1. Experimental setup

In this paper, the experiments were conducted on a 6-bladed automotive engine cooling fan with equal blade pitches. The 6-bladed rotor is located upstream the stator, which contains 19 outlet guide vanes (OGV). Various primary flow conditions have been tested in this paper. In this section, the primary noise arising from the rotor/stator interaction has been slightly increased by adding a small tape (2 cm $\times$ 4 cm) between two stator outlet guide vanes (Fig. 1). An experimental setup has been used to demonstrate that the interaction between the rotor and the upstream control obstructions can generate noise and eventually destructively

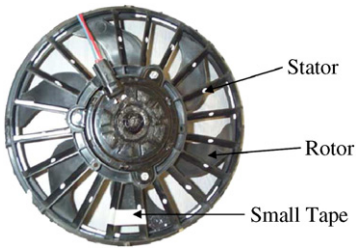

Fig. 1. Rotor/stator + small tape arrangement.

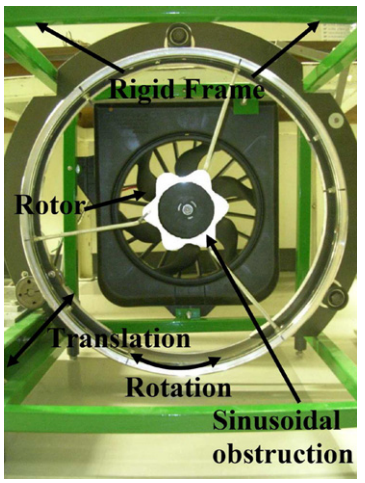

Fig. 2. Experimental setup to study the acoustic radiation resulting from the rotor and the upstream obstruction.

interfere with the primary fan noise, depending on the position and orientation of the obstruction upstream the fan.

Fig. 2 presents the experimental setup used to evaluate the acoustic radiation arising from the interaction between the rotor and the control obstructions (a sinusoidal obstruction is used for illustration). An engine cooling unit (axial fan mounted in a shroud) is installed in a rigid frame, downstream a positioning device allowing for the obstruction to be moved in the axial and angular directions. The fan has six regularly spaced blades and its rotational velocity is 2900 rev/min, corresponding to a BPF at 290 Hz. The internal diameter of the fan is 12.5 cm while its external diameter is 30 cm. The 6-period sinusoidal obstruction shown in Fig. 2 is made of plexiglas and have an inner radius of $R_1 = 5.5$ cm and an outer radius of $R_2 = 7$ cm.

Acoustic pressure measurements were performed in an anechoic room with and without control obstruction to extract the contribution of the obstruction to the total radiated acoustic pressure. An upstream microphone (B&K type 4189 pre-polarized $\frac{1}{2}$ in) was located on the fan axis at a distance of 2 m. The results are averaged over 20 sample blocks with a spectral resolution of 1 Hz between 0 and 2 kHz.

2.2. SPL measurements

The acoustic pressure measurements were conducted at the BPF and its first three harmonics for 651 axial and angular locations of sinusoidal and trapezoidal control obstructions and also from cylindrical obstructions (Fig. 3). In the following, z_s is the axial distance between the rotor and the control obstruction and θ_s is the angular position of the control obstruction. The control obstruction is translated by $\delta_{zs} = 0.5$ cm increments in the axial direction from $z_s = 13.5$ to 8.5 cm, and by $\delta_{zs} = 0.25$ cm increments from $z_s = 8.25$ to 3.5 cm. The control obstruction is rotated by $\delta_{\theta_s} = 3^\circ$ increments over a period of $2\pi/6$ for each axial position.

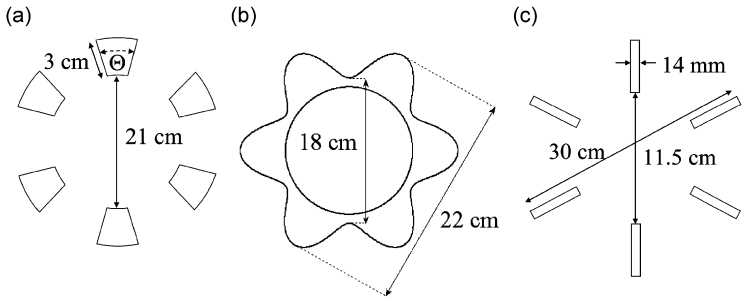

Fig. 3. Geometries of the control obstructions: (a) trapezoidal obstructions, (b) sinusoidal obstruction and (c) cylindrical obstructions.

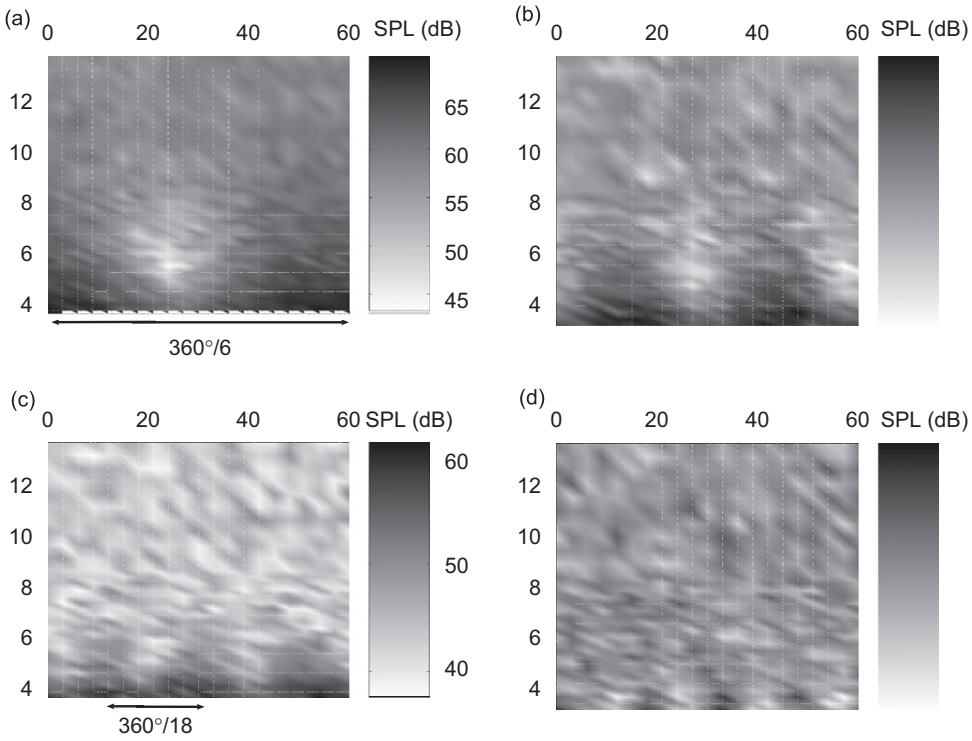

Fig. 4. Sound pressure level as a function of the control obstruction location—6-trapezoidal obstruction ($\Theta = 10^\circ$), leading to a high harmonic content rate. (a) BPF (b) 2 × BPF, (c) 3 × BPF, (d) 4 × BPF.

Fig. 4 shows the SPL at BPF, 2 × BPF, 3 × BPF and 4 × BPF (respectively in Figs. 4a–d) as a function of the axial distance and angular position of a 6-trapezoidal obstruction, for a small angle $\Theta = 10^\circ$, of the trapezoids (see Fig. 3a). It has been checked experimentally that the control obstruction has no effect at $z_s = z_s^{\max}$. Thus, in Fig. 4, the primary sound power level is approximatively given by the average of sound power level at $z_s = z_s^{\max}$. Fig. 4a shows that, to minimize the acoustic pressure level at the BPF, the optimal axial distance between the rotor and the control obstruction is $z_s^{\text{opt}} = 5.25\,\text{cm}$, and the optimal angular position is about $\theta_s^{\text{opt}} = 24^\circ$. In this orientation, the circumferential harmonic of order 6 of the primary unsteady lift is out of phase with the circumferential harmonic of order 6 of the secondary unsteady lift. It can also be seen that, at BPF and for $24^\circ + 360/2 \times 6^\circ = 54^\circ$ orientation, the 6-trapezoidal obstruction creates a secondary acoustic field in phase with that created by the primary rotor/stator interaction.

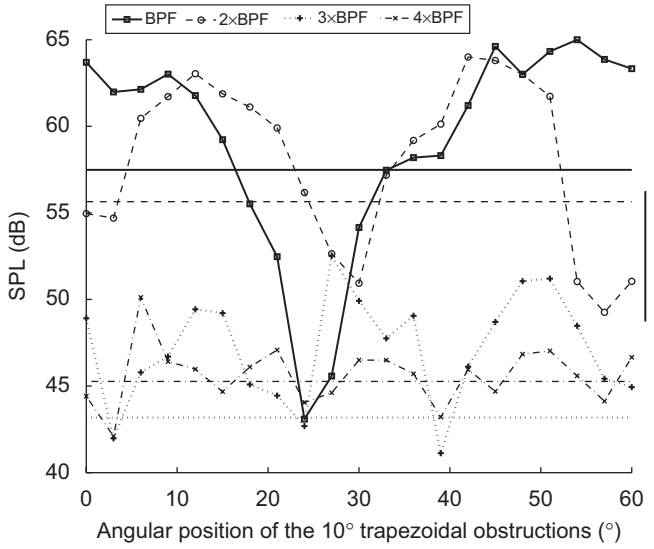

Fig. 5. Sound pressure level produced by the $\Theta = 10^\circ$ 6-trapezoidal obstruction at optimal axial location z_s^{opt}, measured by the upstream on-axis microphone.

In Fig. 5, the primary sound power level are plotted as horizontal lines for the BPF and its first three harmonics. The total sound power level is plotted as a function of the angular position of the control obstruction for the optimal axial distance. The primary acoustic pressure level is increased by about 6 dB when the primary unsteady lift and the secondary unsteady lift are in phase. It validates the assumption of the linear superposition of the two acoustic sound fields in Eq. (6) of Ref. [1]. It has also been verified for all the obstructions shown in this paper. The evolution of the BPF tone as a function of the obstruction orientation is characteristic of an interference pattern.

As seen in Fig. 5 and in Figs. 4b–d, the 6-trapezoidal obstruction also tends to affect the higher order harmonics. For example, in Fig. 4b, the acoustic pressure level measured for the harmonic $2 \times$ BPF varies with an angular period two times shorter than for BPF. The amplitude of the variation of the acoustic pressure level is also smaller than for BPF. These results confirm that a low angle Θ 6-trapezoidal obstruction has a non-negligible contribution to the circumferential order $w = 2B$ of the total unsteady lift, which radiates sound at the frequency $2 \times$ BPF. In Figs. 4(c and d), the acoustic pressure level measured for the harmonic $3 \times$ BPF and $4 \times$ BPF respectively vary with an angular period three times and four times shorter than for BPF, especially at low axial distance z_s. However, these higher harmonics of the BPF seem to be less affected by the 10° 6-trapezoidal obstruction.

2.3. Indirect estimation of the unsteady lift generated by the control obstructions

An indirect estimation of the unsteady lift generated by the control obstructions, based on the SPL measurements previously shown (Fig. 4) is proposed to validate the theoretical results of Ref. [1].

From Figs. 5 and 4, we can see that the $\Theta = 10^\circ$, 6-trapezoidal obstruction affects the harmonics of the BPF (especially its first harmonic). It has also been shown analytically [1], that the circumferential order $w = B$ is not the only circumferential order in the unsteady lift spectrum generated by obstructions. To compare the analytical prediction of the unsteady spectrum generated by the trapezoidal, sinusoidal and cylindrical obstructions, the ratios $\|\tilde{L}_s(B)\|/\|\tilde{L}_s(mB)\|$, are now indirectly estimated from the acoustic pressure level as a function of the control obstruction location, by manipulating Eqs. (7) and (8) of Ref. [1].

By considering the particular case of the sound radiation in the axial direction $\mathbf{x} = (r, 0, 0)$, only the circumferential harmonic mB of the unsteady lift radiates sound at frequency $mB\Omega$ because only the 0th order Bessel function in Eq. (8) of Ref. [1] takes a non-zero value when its argument is zero ($J_0(0) = 1$). Thus, in the

axial direction, the radiation transfer function (Ref. [1, Eq. (8)]) is reduced to $[H(r,0,0;\omega)]_{w=mB} = -(\mathrm{i}mB^2\Omega/4\pi rc_0)\cos\gamma$.

Then, by writing the complex value of the unsteady lift in terms of magnitude and phase: $\tilde{L}_p(w) = L_p(w)\,\mathrm{e}^{\mathrm{i}w\theta_p^L(w)}$ and $\tilde{L}_s(w,z_s,\theta_s) = L_s(w,z_s)/,\mathrm{e}^{\mathrm{i}w\theta_s^L(w,z_s,\theta_s)}$, where $L_p(w)$ and $L_s(w,z_s)$ are, respectively, the magnitude of the circumferential component w of the primary and secondary lift and $\theta_p^L(w)$ and $\theta_s^L(w,z_s,\theta_s)$ are, respectively, the phase of the circumferential component w of the primary and secondary lift, the acoustic pressure at the harmonic m of the BPF (Ref. [1, Eq. (7)]) as a function of the location of the control obstruction (z_s,θ_s) can be written as follows:

$$p_t(r,0,0,mB\Omega,z_s,\theta_s) = -\frac{\mathrm{i}mB^2\Omega}{4\pi rc_0}\cos\gamma \times (L_p(mB)\,\mathrm{e}^{\mathrm{i}mB\theta_p^L(mB)} + L_s(mB,z_s)\,\mathrm{e}^{\mathrm{i}mB\theta_s^L(mB,z_s,\theta_s)}) \tag{1}$$

The dependance of the secondary unsteady lift as a function of the axial distance z_s between the rotor and the control obstruction is formally taken into account in the magnitude $L_s(w,z_s)$ and the phase $\theta_s^L(w,z_s,\theta_s)$ of the unsteady lift. The phase of the secondary unsteady lift also depends on the angular location of the control obstruction θ_s in the following way: $\theta_s^L(w,z_s,\theta_s) = \theta_s + \theta_s^L(w,z_s,0)$. The term $\theta_s^L(w,z_s,0)$ refers to the ability of the phase of the secondary unsteady lift to change as a function of z_s, due to swirl of the flow for example. Such effects of inter-dependence of the magnitude and phase of the secondary noise due to the swirl of the flow has been shown experimentally by Lemke et al. [12] when injecting steady jets to control tonal noise in turbomachines. They observed that the optimal circumferential position varies with the injection rate of oblique jets. No such effect has been observed for the obstructions used in this paper ($\theta_s^L(w,z_s,0) = \theta_s^L(w,z_s^{\mathrm{opt}},0)$), which is of practical interest when adjusting the position of the control obstruction (since, in this case, the change in magnitude and the change in phase of the secondary sound field are not coupled as a function of the axial distance z_s).

A particular case can be pointed out when the angular location of the control obstruction θ_s is chosen such that the primary and secondary unsteady lifts are in phase ($\theta_p^L(mB) = \theta_s^L(mB,z_s,\theta_s)$). In this case, the Eq. (1) can be rearranged to give the following dimensionless ratio:

$$\frac{\|\tilde{L}_s(1B,z_s)\|}{\|\tilde{L}_s(mB,z_s)\|} = m \times \frac{\|p_t(r,0,0;1B\Omega,z_s,\theta_p^L=\theta_s^L)\| - \|p_p(r,0,0;1B\Omega)\|}{\|p_t(r,0,0;mB\Omega,z_s,\theta_p^L=\theta_s^L)\| - \|p_p(r,0,0;mB\Omega)\|} \tag{2}$$

Moreover, the harmonic content rate D, proposed in Ref. [1] to compare the ability of the various obstructions tested in this paper to control the fundamental of the circumferential unsteady lift spectrum without generating upper harmonics in both the unsteady lift spectrum and the acoustic spectrum, can be easily estimated by extracting $\tilde{L}_s(mB,z_s)$ from Eq. (1):

$$D(z_s) = \sqrt{\frac{\sum_{m=2}^{m_{\max}}\|\tilde{L}_s(mB,z_s)\|^2}{\sum_{m=1}^{m_{\max}}\|\tilde{L}_s(mB,z_s)\|^2}} \times 100 \tag{3}$$

The two harmonic content indicators (the ratios $\|\tilde{L}_s(w=1B,z_s)\|/\|\tilde{L}_s(w=mB,z_s)\|$ and the harmonic content rate $D(z_s)$) are estimated for several discretized axial distances $z_{s,i}$ between the rotor and the control obstruction, when the mB periodicity of the sound power level at the harmonic $m\times$ BPF as a function of the angular position of the control obstruction θ_s is clearly visible. In Fig. 4, the indicators are estimated from the optimal location $z_s^{\mathrm{opt}} = 5.25\,\mathrm{cm}$, to the nearest location $z_{sN} = 3.5\,\mathrm{cm}$, where N is the number of discretized axial distance for which the two indicators are calculated. To provide a range of these estimators valid for various axial locations of the control obstructions (thus to control various magnitude of the primary sound pressure), they are averaged over the axial distances z_{sn}. Averaged values and standard deviations are calculated as follows:

$$D = \frac{1}{N}\sum_n D(z_{s,n}) \tag{4}$$

$$\sigma_D = \sqrt{\frac{1}{N}\sum_n (D(z_{s,n}) - D)^2} \tag{5}$$

$$\frac{\|\tilde{L}_s(w = 1B)\|}{\|\tilde{L}_s(w = mB)\|} = \frac{1}{N}\sum_n \frac{\|\tilde{L}_s(w = 1B, z_{s,n})\|}{\|\tilde{L}_s(w = mB, z_{s,n})\|} \tag{6}$$

$$\sigma_{\|\tilde{L}_s(w=1B)\|/\|\tilde{L}_s(w=mB)\|} = \sqrt{\frac{1}{N}\sum_n \left(\frac{\|\tilde{L}_s(w = 1B, z_{s,n})\|}{\|\tilde{L}_s(w = mB, z_{s,n})\|} - \frac{\|\tilde{L}_s(w = 1B)\|}{\|\tilde{L}_s(w = mB)\|}\right)^2} \tag{7}$$

In this paper, the indicators are presented as the averaged value D (or $\|\tilde{L}_s(w = 1B)\|/\|\tilde{L}_s(w = mB)\|$) $\pm$ the standard deviation σ_D (or $\sigma_{\|\tilde{L}_s(w=1B)\|/\|\tilde{L}_s(w=mB)\|}$).

The first effect of the averaging over the axial distance z_s is to minimize the effect of random uncertainties on the two indicators. The second effect of the averaging over the axial distance z_s is to eventually average a deterministic variation of the wake width (as a function of z_s) generated by the obstruction upon the two indicators. Indeed, the wake disturbance velocity impinging the rotor blades can be sharper for low axial distance z_s [16], thus increasing the contribution of the circumferential harmonics contained in the unsteady lift spectrum. Thus $D(z_s)$ increases and $\|\tilde{L}_s(w = 1B, z_s)\|/\|\tilde{L}_s(w = mB, z_s)\|$ decreases when decreasing z_s.

2.4. Effect of the wake width generated by 6-trapezoidal obstructions

Several trapezoidal obstruction angles $\Theta = [10^\circ, 20^\circ, 30^\circ, 35^\circ, 40^\circ, 50^\circ]$ were experimentally tested to verify the analytical prediction shown in Fig. 9 of Ref. [1]. The sound power level at BPF, 2 × BPF, 3 × BPF and 4 × BPF as a function of the location of the 10° trapezoidal obstruction is shown in Fig. 4. The sound power level at the first four tones as a function of the location of the other trapezoidal obstructions ($\Theta = [20^\circ, 30^\circ, 35^\circ, 40^\circ, 50^\circ]$) were also measured to estimate the harmonic content indicators following the procedure described in Section 2.3.

Since no anemometric measurements were carried out for the trapezoidal obstructions, the Gaussian width parameter $a = 0.5$, has been imposed in Fig. 6 to compare the measured values of the harmonic content rate $D(\%)$ and the ratio $\|\tilde{L}_s(w = 1B)\|/\|\tilde{L}_s(w = 2B)\|$, to the analytical predictions. The error bars correspond to $\pm$ one standard deviation around the averaged values of the harmonic content indicators, as explained in Section 2.3. The experimental estimations of the harmonic content rate and the ratio $\|\tilde{L}_s(w = 1B)\|/\|\tilde{L}_s(w = 2B)\|$, are in good agreement with the analytical predictions when imposing a Gaussian wake parameter $a_R = 0.5$, for the radial dependence of the inflow velocity magnitude in the analytical modeling, as shown in Eq. (24) of Ref. [1]. The radial wake width coefficient $a_R = 0.5$, was estimated from hot wire anemometer measurements behind a sinusoidal obstruction. Since the radial extent of the trapezoidal obstructions used in this section is approximatively equal to the radial extent of the sinusoidal obstruction, $a_R = 0.5$ is expected to be accurate for trapezoidal obstructions. When no Gaussian distribution in the radial direction is included in the analytical model ($a_R \to \infty$), the differences are quite large but trends are similar to the experimental estimations of $D(\%)$ and the ratio $\|\tilde{L}_s(w = 1B)\|/\|\tilde{L}_s(w = 2B)\|$ (see Fig. 6). It can be seen that the standard deviations associated to the ratios $\|\tilde{L}_s(w = 1B)\|/\|\tilde{L}_s(w = 2B)\|$, is high for the trapezoidal obstructions with a low harmonic content rate: for $\Theta = 35^\circ$, the high standard deviation is due to the random uncertainties of the two indicators and for $\Theta = 40^\circ$, the high standard deviation is associated to a monotonic decrease of the ratio $\|\tilde{L}_s(w = 1B, z_s)\|/\|\tilde{L}_s(w = 2B, z_s)\|$, as a function of z_s.

The differences between the experimental estimations and the analytical predictions originate from several approximations in the analytical modeling, as explained in Ref. [1] and from uncertainties in the acoustic pressure measurements, especially the non-stationary part of the BPF tone and its harmonics. Another source of uncertainty in the measurement comes from the discretization of the angular location θ_s of the control obstruction, which can lead to an under-estimation of $\|p_t(r, 0, 0; mB\Omega, z_s, \theta_p^L = \theta_s^L)\|$ so that the ratio defined in Eq. (2) is corrupted by uncertainties. The averaging effects over the axial distance z_s are included in the error bars, as explained in Section 2.3.

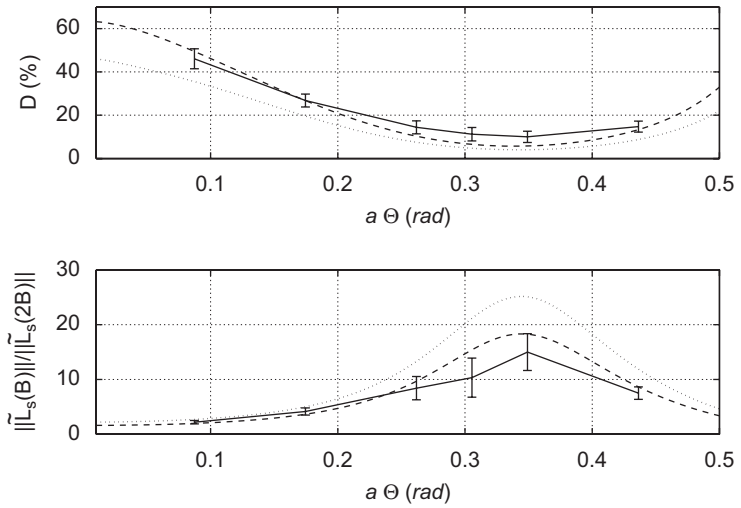

Fig. 6. Harmonic content indicators, associated to the circumferential unsteady lift spectrum generated by 6-trapezoidal obstructions, as a function of the product $a\Theta$ for an actual automotive fan. Top: harmonic content rate D (%), bottom: ratio between the fundamental unsteady lift order and its first harmonic $\|\tilde{L}_s(w=1B)\|/\|\tilde{L}_s(w=2B)\|$. Solid line: estimated from acoustic pressure measurements by imposing $a=0.5$, dashed line: analytically prediction $a_R=0.5$, dotted line: analytically predicted $a_R\to\infty$.

As anticipated analytically in Ref. [1], salient wakes generated by low width obstructions lead to a large harmonic content rate of the unsteady lift, thus leading to a risk of affecting the harmonics of the BPF. Better obstructions can be designed thanks to the analytical modeling presented in part I [1], to minimize the harmonic content rate of the unsteady lift. For example, the angles $\Theta=[30^\circ,35^\circ,40^\circ,50^\circ]$, of the 6-trapezoidal obstruction lead to a low harmonic content rate. The angle $\Theta=40^\circ$, of the trapezoids provides the lowest harmonic content rate and the highest ratio between the fundamental of the unsteady lift spectrum and its first harmonic. The optimal angular wake width is $a\Theta=0.5\times40^\circ=20^\circ$. This angle is about 10° greater than the angular portion occupied by the blades at mid-span.

2.5. Harmonic content indicators for a sinusoidal obstruction

Fig. 7 shows the sound power level of the first four tones as a function of sinusoidal obstruction location. As expected, the sinusoidal obstruction has a strong influence on the BPF magnitude as a function of its location (Fig. 7a). The sinusoidal obstruction also affect the $2\times$ BPF tone (Fig. 7b) but has a negligible effect at frequency $3\times$ BPF (Fig. 7c) and $4\times$ BPF (Fig. 7d). The estimated values of the ratios $\|\tilde{L}_s(w=1B)\|/\|\tilde{L}_s(w=mB)\|$, calculated from the acoustic pressure measurements of Fig. 7 and the Eq. (2), are given in Table 1 for $1\leqslant m\leqslant4$, for the sinusoidal obstruction shown in Fig. 3b. The energy contained in the first circumferential harmonic of the unsteady lift is non-negligible, but the upper harmonics decrease rapidly. The order of magnitude of the ratio $\|\tilde{L}_s(w=1B)\|/\|\tilde{L}_s(w=mB)\|$, estimated by indirect acoustical pressure measurements is similar to the semi-analytical predictions of Ref. [1]. The term "semi"-analytical is used since the wake velocity profile has been measured behind the obstruction using a single hot wire anemometer. A Gaussian approximation of the measured velocity profile has then been used as input data in the analytical model [1] to estimate the circumferential spectrum of the unsteady lift generated by the sinusoidal obstruction. Apart from the approximations of the analytical modeling (e.g. only transversal gust are considered in the Sears theory), the differences between the semi-analytical predictions and the indirect experimental estimations of the indicators originate from the hot-wire measurements and from the gaussian approximation of the velocity profile generated by the sinusoidal obstruction. The uncertainties can also originate from uncertainties in the acoustic pressure measurements, i.e. from the non-stationary part of the acoustic radiation or from the discretization effect of the angular position of the control obstruction and from the averaging over z_s, as explained in Section 2.4.

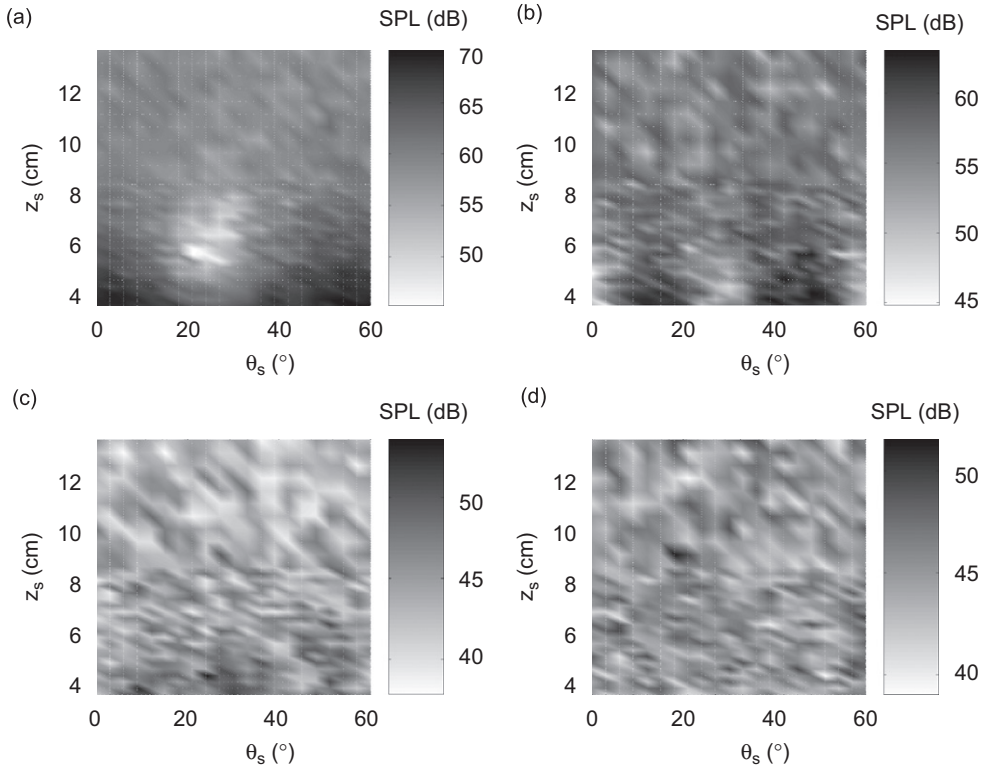

Fig. 7. Sound pressure level as a function of the control obstruction location—sinusoidal obstruction: (a) BPF, (b) 2 × BPF, (c) 3 × BPF and (d) 4 × BPF.

Table 1
Indirect estimation of the ratio $\|\tilde{L}_s(w=1B)\|/\|\tilde{L}_s(w=mB)\|$, from acoustical measurement in the axial direction for the sinusoidal obstruction

m	1	2	3	4
Estimated from acoustical pressure measurements	1	6.5±1	35.0±5.7	–
Calculated from the analytical model [1] and hot wire anemometer data	1	5.3	39.6	342

No value was experimentally estimated for the ratio $\|\tilde{L}_s(w=1B)\|/\|\tilde{L}_s(w=4B)\|$, since no periodicity of the acoustic pressure level as a function of the angular position of the sinusoidal obstruction θ_s was found at frequency 4 × BPF, even for low axial distance z_s between the rotor and the control obstruction. Finally, the semi-analytical prediction of $D=18.1\%$, calculated in Ref. [1] is in the range of the indirect experimental estimation $D=17.8\%\pm2.8\%$.

2.6. Harmonic content indicators for a 6-cylindrical obstructions

Finally, cylindrical obstructions are tested to compare the harmonic selectivity of the proposed obstructions to the cylindrical obstructions used in the literature [7–11]. The diameter of the tested cylinders is 14 mm. Fig. 8 shows the sound power level of the first four tones as a function of the 6-cylindrical obstruction position. The cylinders has a strong influence at BPF (Fig. 8a), but also at 2 × BPF (Fig. 8b) and at 3 × BPF (Fig. 8c). Small influence is noted at 4 × BPF (Fig. 8c). A larger range of axial distance between the rotor and

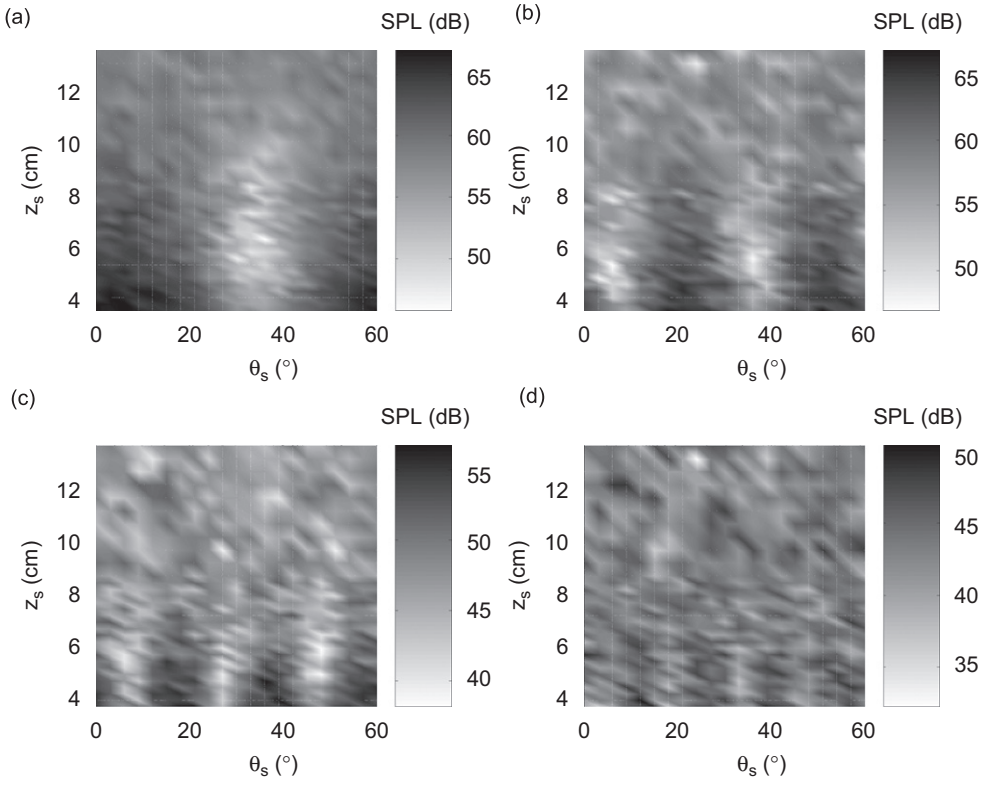

Fig. 8. Sound pressure level as a function of the control obstruction location—cylindrical obstructions (14 mm diameter): (a) BPF (b) 2 × BPF, (c) 3 × BPF and (d) 4 × BPF.

Table 2
Indirect estimation of the ratio $\|\tilde{L}_s(w=1B)\|/\|\tilde{L}_s(w=mB)\|$, from acoustical measurement in the axial direction for the cylindrical obstructions

m	1	2	3	4
Estimated from acoustical pressure measurements	1	2.8±0.2	13.1±2.0	–
Calculated from the analytical model [1] ($a=0.5$)	1	1.7	2.8	5.0
Calculated from the analytical model [1] ($a=1$)	1	2.9	11.3	59.0

the cylindrical obstructions for which the BPF is reduced (Fig. 8a) is observed compared to the trapezoidal (Fig. 4a) and the sinusoidal obstructions (Fig. 7a).

The ratios $\|\tilde{L}_s(w=1B)\|/\|\tilde{L}_s(w=mB)\|$, indirectly estimated from the acoustic pressure level measurements of Fig. 8 and Eq. (2) are shown in Table 2. The ratio $\|\tilde{L}_s(w=1B)\|/\|\tilde{L}_s(w=2B)\|=2.8$, indicates that the cylinders have a non-negligible effect on the 2 × BPF tone. The magnitude of the second harmonic of the circumferential spectral order of the unsteady lift is 13.1 times smaller than the fundamental order. The ratio $\|\tilde{L}_s(w=1B)\|/\|\tilde{L}_s(w=4B)\|$, could not be estimated from the sound pressure data.

The experimentally estimated ratios $\|\tilde{L}_s(w=1B)\|/\|\tilde{L}_s(w=mB)\|$, are compared to the analytical prediction of Ref. [1] by considering that the one-dimensional Gaussian wake model is identical for rectangular and cylindrical obstructions. The prediction and measurement are in quite good agreement for a Gaussian wake width parameter $a=1$, but large differences can be pointed out for $a=0.5$. The harmonic content rate estimated from the acoustic pressure measurements is $D=37.6\%\pm2.3\%$, which is close to the analytically predicted value $D=33.5\%$, for the large wake width parameter $a=1$ but diverge for $D=58.6\%$, calculated

from the analytical modeling by choosing $a = 0.5$. Thus, an a priori unexpected application of the method to estimate the harmonic content indicators is the indirect estimation of the Gaussian wake width characteristic, behind an obstruction in the flow field of a rotor, from acoustical pressure measurements using a single microphone in the axial direction and by varying the angular position of the obstruction.

3. Directivity and sound power attenuation in free field

After analyzing the harmonic selectivity of the trapezoidal, sinusoidal and cylindrical obstructions, the spatial performance of the flow control obstruction approach is illustrated in acoustic free field conditions. Acoustic pressures are measured to determine the acoustic directivity and sound power attenuations in both the upstream and downstream half-spaces for two primary noise conditions.

3.1. Experimental setup

The experimental setup presented in Fig. 2 is now used to measure the far-field acoustic directivity at BPF for the fan with and without control obstruction. The control is performed using the sinusoidal obstruction presented in Fig. 3b. The sinusoidal obstruction is located upstream. Acoustic pressure measurements are performed in an anechoic room on 1.8 m radius hemispheres upstream and downstream the fan. The acoustic pressures are measured at 33 regularly spaced locations on each hemisphere. The directivity patterns are obtained for two primary flow conditions: (i) flow non-homogeneity arising from the interaction between the rotor and the stator outlet guide vanes (Fig. 9a), for which the optimal distance between the sinusoidal obstruction and the rotor is $z_s^{\mathrm{opt}} = 6\,\mathrm{cm}$ and (ii) flow non-homogeneity arising from the interaction between the rotor, the stator outlet guide vanes and a triangular obstruction in order to increase flow non-homogeneity (Fig. 9b). The triangular obstruction was inserted between two vanes of the stator. This obstruction covers a 34° angular section and strongly interacts with the rotor. This obstruction tends to increase the amplitude of the BPF in the acoustic spectrum as it introduces energy in the low-order circumferential components of the unsteady lift [15]. For this primary flow condition (case (ii)), the optimal distance between the sinusoidal obstruction and the rotor is $z_s^{\mathrm{opt}} = 4.5\,\mathrm{cm}$, which is lower than the optimal distance for controlling the weaker interaction (case (i)) between the rotor and the stator outlet guide vanes.

3.2. Control of the primary noise generated by rotor/stator interaction

Fig. 10 presents the upstream and downstream sound pressure frequency spectra, at 1.8 m on the fan axis for the case (i) of rotor/stator primary interaction. The control obstruction is effective at BPF but tends to slightly increase the broadband noise floor. At BPF, the attenuations are 12.2 dB for upstream and downstream on-axis sound pressure. The impact of the sinusoidal obstruction on sound radiation at BPF harmonics is small, which confirm the frequency selectivity of a sinusoidal obstruction. In Fig. 10, the increase in the broadband energy arises from vortex generated by the sharp edges of the obstruction which then impact the fan blades, producing random fluctuating forces. The broadband noise is only increased when the primary inflow is

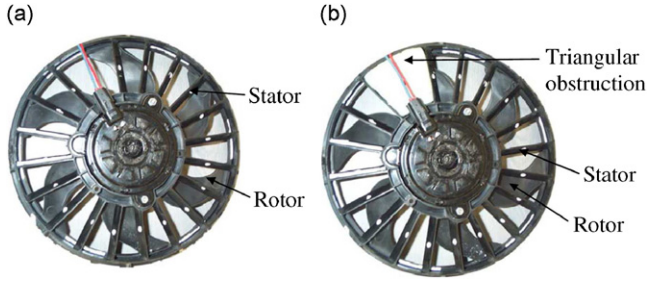

Fig. 9. Picture of the rotor/stator arrangement (left) and Rotor/stator + triangular obstruction arrangement (right): (a) rotor/stator, case (i) and (b) rotor/stator + triangular obstruction, case (ii).

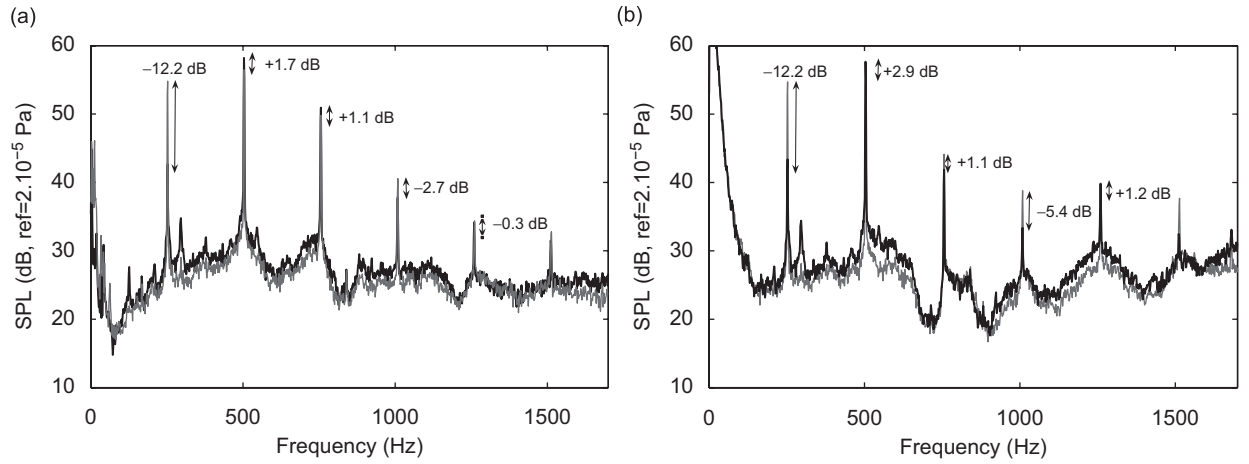

Fig. 10. Sound pressure spectrum with (black thick line) and without sinusoidal flow obstruction (gray thin line) for the case (i) of rotor/stator interaction: (a) upstream microphone and (b) downstream microphone.

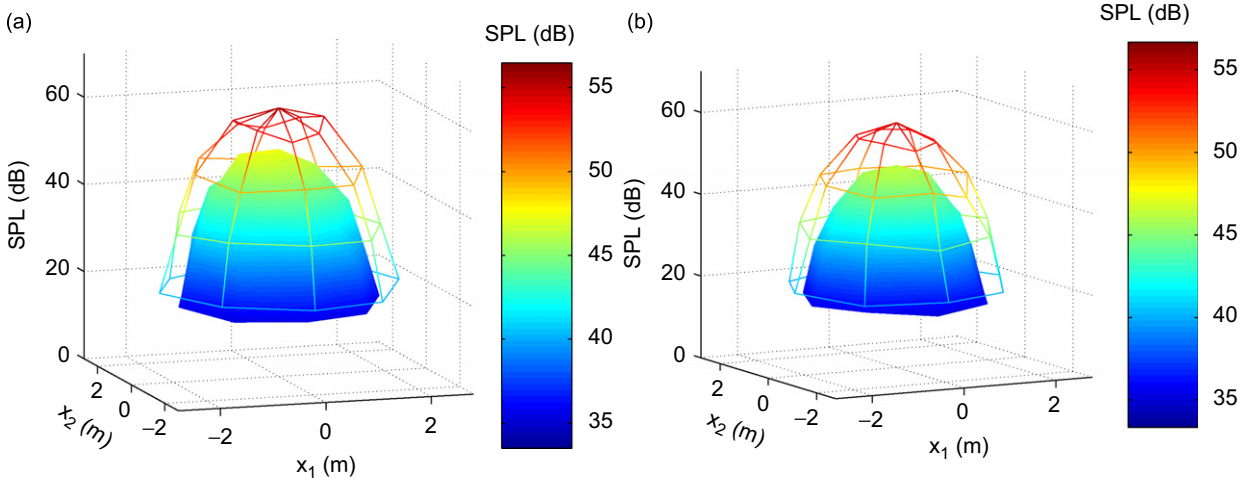

Fig. 11. (a) Upstream and (b) downstream directivity at BPF in free field for the case (i) of rotor/stator interaction. Without sinusoidal control obstruction (lines) and with sinusoidal control obstruction (surfaces).

relatively clean, but when a radiator is installed in the upstream flow field, no amplification of the broadband noise is noted.

The acoustic directivity with and without control obstruction is presented in Fig. 11 for the case (i) of rotor/stator interaction. It appears that an acoustic attenuation is obtained in the whole radiating space and the attenuation is almost the same upstream and downstream. The most radiating circumferential order $B = 6$, of the unsteady lift is effectively controlled, so that the attenuation is larger in the axial direction.

The sound power attenuations, defined as $10\log_{10}(W_p(m)/W_t(m))$, where $W_p(m)$ is the primary sound power and $W_t(m)$ is the total sound power at frequency $mB\Omega$, are presented in Table 3 for the case (i) of rotor/stator primary interaction. The sound power attenuation is 8.4 dB in both the upstream and the downstream half-spaces at BPF. In this case, the flow is spatially slightly non-uniform. Sound power attenuation or amplification is negligible for the first three harmonics of the BPF.

Table 3
Acoustic power attenuation for the case (i) of rotor/stator primary interaction

$m \times$ BPF	1×BPF	2 × BPF	3 × BPF	4 × BPF
Downstream	+8.4	0	−1.1	+0.4
Upstream	+8.4	−0.9	−0.6	0

$10\log_{10}(W_p(m)/W_t(m))$.

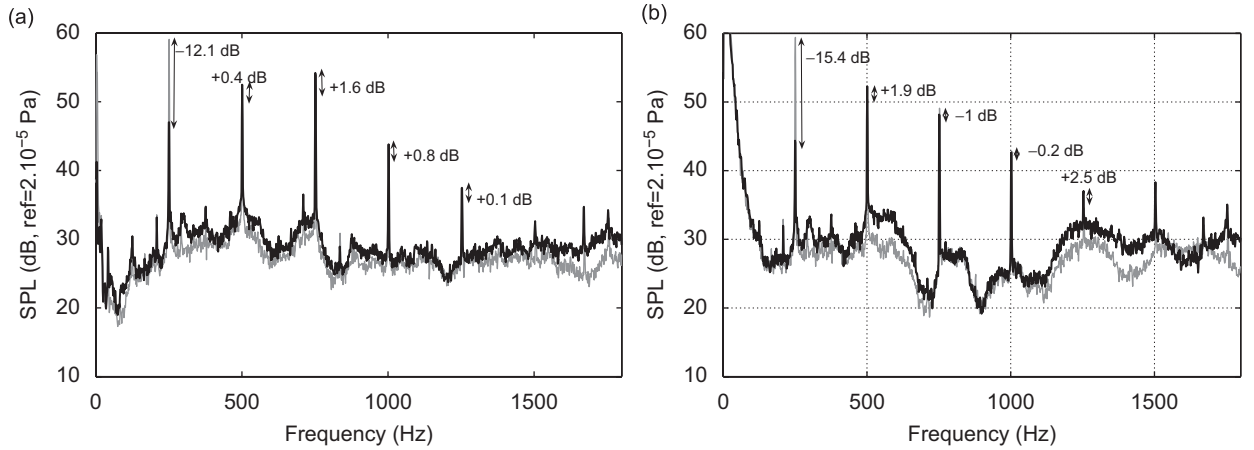

Fig. 12. Sound pressure spectrum with (black thick line) and without sinusoidal flow obstruction (gray thin line) for the case (ii) of rotor/(stator and triangular obstruction) interaction: (a) upstream microphone and (b) downstream microphone.

3.3. Control of the amplified primary noise generated by rotor/(stator + triangular obstruction) interaction

Fig. 12 presents the upstream and downstream sound pressure frequency spectra, at 1.8 m on the fan axis for the case (ii) of rotor/(stator plus triangular obstruction) primary interaction. The control obstruction is effective at BPF but tends to slightly increase the broadband noise floor, but, as noted for the case (i) interaction (Section 3.2), when a radiator is installed in the upstream flow field, no amplification of the broadband noise is noted. At BPF, the attenuations are in the order of 10–20 dB for upstream and downstream on-axis sound pressure. The impact of the sinusoidal obstruction on sound radiation at BPF harmonics is small, which confirm the frequency selectivity of a sinusoidal obstruction.

The acoustic directivity with and without control obstruction is presented in Fig. 13 for the case (ii) of rotor/(stator + triangular obstruction) interaction. It appears that an acoustic attenuation is obtained in the whole radiating space. The most radiating circumferential order $B = 6$ of the unsteady lift is effectively controlled, so that the attenuation is particularly large in the axial direction. Contrary to the control of the primary noise generated by the rotor/stator interaction (case (i)), the control is not as effective downstream and upstream for the primary noise generated by the rotor/(stator + triangular obstruction) interaction (case (ii)). As shown in Table 4, at BPF, the sound power is attenuated by 7 dB in the upstream half-space and 2.6 dB in the downstream half-space when a triangular obstruction is added between two stator vanes (case (ii)), which generate a spatially highly primary non-uniform flow. The variation of sound power is negligible for the harmonics of the BPF, as noted in Fig. 12 in the axial direction.

Depending on the primary noise (case (i) or case (ii)), the sound power attenuation is not the same in the upstream half-space and in the downstream half-space. We also experimentally observed that there is a trade-off between an optimal control in the downstream and in the upstream radiating half-spaces. This can be done by slightly adjusting the axial distance between the control obstruction and the rotor. An axial variation of about 1 cm can result in a maximal attenuation at the BPF in the downstream half-space or a maximal

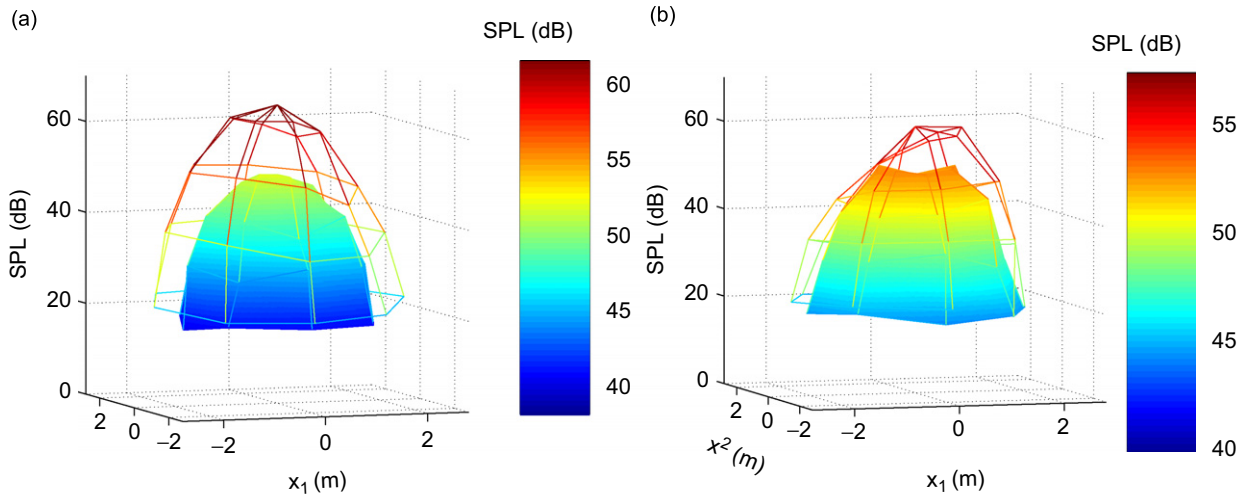

Fig. 13. (a) Upstream and (b) downstream directivity at BPF in free field for the case (ii) of rotor/(stator and triangular obstruction) interaction. Without sinusoidal control obstruction (lines) and with sinusoidal control obstruction (surfaces).

Table 4
Acoustic power attenuation for the case (ii) of rotor/(stator plus triangular obstruction) primary interaction $10\log_{10}(W_p(m)/W_t(m))$

$m \times$ BPF	$1 \times$ BPF	$2 \times$ BPF	$3 \times$ BPF	$4 \times$ BPF
Downstream	+7	−1.5	+0.9	−0.2
Upstream	+2.6	−0.7	−0.6	+0.1

attenuation at the BPF in the upstream half-space. Intermediate axial positions allow for the tonal noise to be equally attenuated in both the downstream and the upstream half-space.

4. Aerodynamic performance of the fan with a control obstruction

4.1. Experimental setup

The impact of a trapezoidal obstruction (Fig. 3a) and a sinusoidal obstruction (Fig. 3b) on the aerodynamic performance of the fan is studied in this section. In order to evaluate this, the experimental facilities of Siemens VDO in London (Ontario, Canada), following the Air Movement and Control Association standard, was used. This setup is made of plenum chambers separated by grids and nozzles in order to allow precise pressure and flow measurement. Fig. 14 presents an overview of the setup. The fan is hermetically inserted between two chambers. The upstream chamber is at atmospheric pressure and the downstream chamber is completely sealed. A hatch located downstream the nozzles allows to adjust the load on the fan. A blower is used to measure the efficiency of the tested fan under forced flow condition, which allows to simulate the operation of an engine cooling fan on an automobile travelling at velocities up to 100 km/h.

The efficiency of the fan is defined as

$$\text{Efficiency} = \frac{\text{Static pressure (Pa)} \times \text{Flow (m}^3\,\text{s}^{-1})}{\text{Input electrical power (W)}} \tag{8}$$

Thus, measurements of static pressure, flow and electrical power are required. The static pressure is measured with the help of Pitot tube located inside the downstream chamber. The flow is obtained from the pressure measured by the Pitot tubes using calibrated nozzles (from differential pressure measurements upstream and

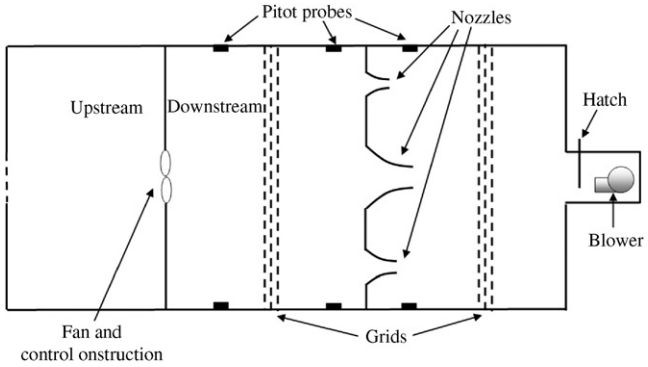

Fig. 14. Experimental setup for the aerodynamic performance evaluation.

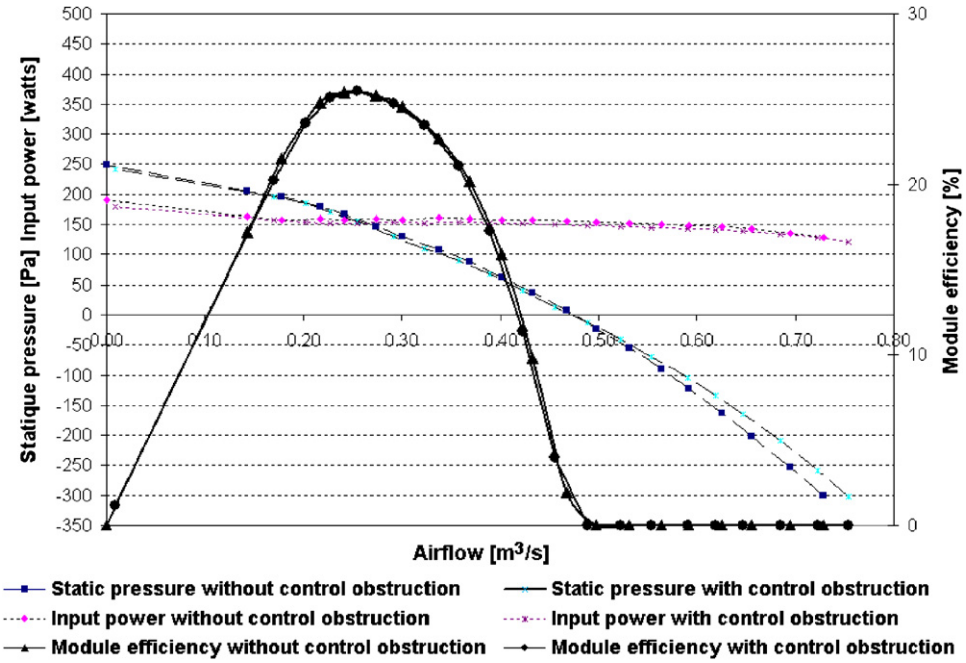

Fig. 15. Aerodynamic performance curves for the fan with the sinusoidal obstruction.

downstream the nozzles). Finally, the electrical power is estimated from voltage and current driving the fan under testing.

4.2. Impact of a control obstruction on the aerodynamic performance of the fan

Fig. 15 presents the static pressure, the input electrical power and the efficiency as a function of the flow, for the fan with and without the sinusoidal obstruction located at the axial control location (4.3 cm from the rotor plane). The effect of the obstruction (the area of this obstruction is 121 cm^2 and the area of the rotor is 707 cm^2) seems almost negligible on the static pressure, the flow and the efficiency of the fan. Larger control obstructions have been tested. It has been shown that a sinusoidal obstruction with a larger area of 196 cm^2, located on the radiator (3 cm from the rotor plane) decreases the maximum efficiency from 25.8% to 24.7%.

Experiments on the fan without radiator also showed that the control obstruction has almost no effect on the fan efficiency, even for a low axial distance between the fan and a 196 cm^2 sinusoidal control obstruction.

Moreover, 12-lobed obstruction (170 cm^2) and 6-trapezoidal obstructions (129 cm^2) similarly have also almost no effect on the fan efficiency.

5. Conclusion

A passive approach has been proposed to reduce tonal noise from axial fan, by controlling the most radiating unsteady lift mode using optimized flow control obstruction(s) with a low harmonic content rate. The flow control obstruction is located such that the secondary radiated noise is of equal magnitude but opposite in phase compared to the primary noise. The magnitude and phase of the secondary noise are respectively controlled by the axial distance between the rotor and the obstruction and the angular position of the control obstruction.

In the paper [1], we provided analytical tools to design the flow control obstructions in order for the blade unsteady lift generated by the rotor/control obstruction interaction to mainly contain the most radiating mode. It has been found that salient obstructions, such as low diameter rods, are not adapted to control a tone without affecting its harmonics; since the circumferential harmonic content of the associated unsteady lift is high. But it is possible to design trapezoidal or sinusoidal control obstructions such that the circumferential harmonic content of the unsteady lift is low. Thus, it is possible to control one tone without affecting its harmonics.

In this paper, we have validated the analytical model presented in Ref. [1] by indirect estimations of the harmonic content indicators from acoustic pressure measurements. Then, free field experiments have shown the ability of the sinusoidal obstruction to control the BPF tone in the whole space. Moreover, the aerodynamic performances of the automotive fan used in this study are almost unaffected by the presence of the control obstruction.

The proposed approach is well adapted to acoustically compact fans, for which only one unsteady lift mode has a major contribution to the radiated noise at a single frequency. Increasing the rotation Mach number and/or the radius of the fan leads to an increase of the number of the radiating unsteady lift modes contributing the noise at a single frequency. It is possible to simultaneously reduce these other modes by adding several obstructions, circumferentially designed to contain the other radiating modes. In such a case, aerodynamic penalties could be of major concern. Therefore, the control approach is better adapted to small industrial chimney fans, PC fans, air conditioning fans, residential heat pump, automotive fans, etc.

Further work involves implementing a feedback control system in order to automatically adjust the obstruction to its optimal solution; and eventually to control time-varying primary flow conditions, which cause the tonal noise to change in magnitude and phase as a function of time. A microphone or embedded sensors could be used to provide the error signal to be minimized. Further effort must also focus on the optimization of aerodynamic shape of the flow control obstructions.

Acknowledgments

This work has been supported by the AUTO21 Network of Centres of Excellence (Canada) and Siemens VDO Automotive Inc. The authors wish to thank Sylvain Nadeau formerly from Siemens Automotive Inc. and Marc Quiquerez for their collaboration to this research.

References

[1] A. Gérard, A. Berry, P. Masson, Y. Gervais, Modelling of tonal noise control from subsonic axial fans using flow control obstructions, *Journal of Sound and Vibration* (2008), this issue, doi:10.1016/j.jsv.2008.09.027.

[2] W. Neise, Review of fan noise generation mechanisms and control methods, *Proceedings of Fan Noise 92*, Senlis, France, 1992, pp. 45–56.

[3] A. Gérard, A. Berry, P. Masson, Control of tonal noise from subsonic axial fan. Part II: active control simulations and experiments in free field, *Journal of Sound and Vibration* 288 (4–5) (2005) 1049–1075.

[4] K.G. Gee, S.D. Sommerfeldt, Application of theoretical modeling to multichannel active control of cooling fan noise, *Journal of the Acoustical Society of America* 115 (1) (2004) 228–236.

[5] C.A. Gerhold, Active control of fan-generated tone noise, *American Institute of Aeronautics and Astronautics Journal* 35 (1) (1997) 17–22.
[6] P.A. Nelson, Active techniques and their potential for application in aeroacoustics, Keynote lecture, *Sixth AIAA/CEAS Aeroacoustic Conference*, Lahaina, Hawaï, 2000.
[7] V. Kota, M.C.M. Wright, Wake generator control of inlet flow to cancel flow distortion noise, *Journal of Sound and Vibration* 295 (2006) 94–113.
[8] C. Polascek, F. Desbois-Lavergne, Fan noise interaction reduction using a wake generator: experiments ans computational aeroacoustics, *Journal of Sound and Vibration* 265 (2003) 725–743.
[9] L. Neuhaus, J. Schulz, W. Neise, M. Möser, Active control of the aerodynamic performance and tonal noise of axial turbomachines, *Proceedings of the Institution of Mechanical Engineers* 217 (2003) 375–383.
[10] K.J. Farrell, S.G. Walter, Technique for reducing acoustic radiation in turbomachinery, *Patent No. US 6,375,416*, April 23, 2002.
[11] A.O. Andersson, Active control of tone noise in engine ducts, *Patent No. PCT/US95/09999 (WO 96/03585)*, February 8, 1996.
[12] O. Lemke, W. Neise, M. Moser, L. Enghardt, Control of higher-order modes at blade passage frequency harmonics of axial turbomachines by steady air jet actuation, *Fan Noise 2007*, Lyon, France, 2007.
[15] A. Gérard, A. Berry, P. Masson, Y. Gervais, Evaluation of tonal aeroacoustic sources in subsonic fans using inverse models, *American Institute of Aeronautics and Astronautics Journal* 45 (1) (2007) 98–109.
[16] M.E. Goldstein, *Aeroacoustics*, McGraw-Hill Inc., New York, USA, 1976.